Interaction of Carbon Monoxide with Anatase Surfaces at High Temperatures: Optimization of a Carbon Monoxide Sensor

Prabir K. Dutta,*,† Arwa Ginwalla,† Brian Hogg,† Bruce R. Patton,‡ Brian Chwieroth,‡ Zheng Liang,§ Perena Gouma,§ Mike Mills,§ and Sheikh Akbar§

Center for Industrial Sensors and Measurements, The Ohio State University, 2041 College Road, Columbus, Ohio 43210-1178

Received: November 18, 1998; In Final Form: March 26, 1999

Sensing the presence of particular gases in harsh environments, such as at high temperatures, poses challenges in the choice of materials as well as in measurements of the appropriate sensing-related property of the material. In this study, we examine the sensing of carbon monoxide (CO) in a nitrogen background at temperatures up to 600 °C using the anatase phase of TiO_2 as the sensing material. In particular, the change in resistance of anatase is used to detect the presence of CO. Copper oxide (CuO) is added to anatase to increase the sensitivity toward CO detection. However, the presence of CuO led to partial transformation of anatase to rutile at temperatures of 800 °C used for bonding the sensor material to the sensing platform. By adding La_2O_3 to the CuO/anatase, the anatase phase is maintained under all thermal treatments. Diffuse reflectance infrared spectroscopy is used to examine the mechanism of CO oxidation. Interaction of lanthanum with the anatase increased the reactivity of the anatase surface toward CO. In addition, the presence of CuO led to increased adsorption of CO as well as enhanced desorption of CO_2, explaining the enhancement of the sensitivity of the CuO-containing anatase toward sensing of CO. Electron microscopy has provided information on the microstructure of the sensor material. An effective medium approximation theory is used to model the observed resistivity data over the temperature range 400−600 °C. The energies of adsorption of CO and the reaction of CO with adsorbed oxygen to form CO_2 are extracted. These values are consistent with the role of CuO acting as a catalyst. This study demonstrates that anatase doped with lanthanum along with the presence of surface/CuO is an effective sensor for CO at temperatures as high as 600 °C.

Introduction

The interaction of gases with transition metal oxide surfaces continues to be an active area of research, primarily stemming from the use of metal oxides as catalysts[1] and sensors.[2] Redox chemistry at oxide surfaces is responsible for processes involving selective oxidation of a variety of organic molecules.[1] Measurement of the resistance of metal oxides is used in the sensing of gases such as CO, H_2, and hydrocarbons and typically involves the chemical reaction of these gases with adsorbed oxygen on the surface.[2] In catalysis and sensing applications, the presence of low levels of other elements on the metal oxide can profoundly influence product formation as well as the sensing behavior.

The most extensively used semiconducting oxide for low-temperature (below 300 °C) gas sensors is SnO_2.[3] The resistance of SnO_2 changes in the presence of combustible gases such as CO, H_2, and CH_4. There is considerable interest in extending the sensing behavior of semiconducting oxides to higher temperatures, particularly for monitoring combustion processes and exhaust, as typified by the needs of the automobile industry.[4] While considerable research has been done on development of metal oxides for low-temperature sensing applications,[5] only few reports are available for gas sensors in harsher environments.[6,7] Previous work from this group has shown that resistance measurements of titania-based systems offer considerable promise for high-temperature sensing of CO.[8] Other reports on TiO_2 as a sensor material includes detection of oxygen for air/fuel control in automobiles.[6,9,10] and as a H_2 detector.[11]

In this report, we focus on ways to improve the sensitivity of TiO_2 as a high-temperature (∼600 °C) CO sensor by modifying the surface with catalysts. It is well established that sensitivity of metal oxide sensors can be improved by addition of noble metals, e.g., Pd and Pt enhances CO sensitivity for SnO_2 sensors.[3] The improvement of the sensing behavior is proposed to arise from catalysis of the CO oxidation reaction. A specific mechanism, titled the "spillover" effect, suggests that the metal catalyst provides sites for adsorption of gas molecules that diffuse onto the SnO_2 surface and become oxidized.[12]

We examine here the sensing of CO on a CuO/titania system, with the intent of using CuO as an oxidation catalyst to promote the CO detection sensitivity. Several metal oxides are known to be active catalysts for oxidation of CO, including oxides of Cu, Cr, Ni, Fe, and Mn.[13] Typically, the oxide catalysts are supported on substrates that maximize the dispersion of the catalyst. In this regard, it has recently been shown that copper oxide on titania is an excellent catalyst for CO oxidation, better than oxides of Co, Mn, and Fe.[14] This was the basis of our choice for examining if the CuO/TiO_2 system would improve the sensing characteristics of CO over that previously reported for TiO_2.[8] There are three phases of TiO_2: anatase, rutile, and brookite, with rutile being the thermodynamically stable phase.[15]

* To whom correspondence should be addressed at Department of Chemistry, The Ohio State University, Columbus, OH 43210.
† Department of Chemistry.
‡ Department of Physics.
§ Department of Materials Science and Engineering.

10.1021/jp9844718 CCC: $18.00
Published on Web 04/29/1999

Since earlier studies have shown that selective oxidation of organics is more pronounced on anatase,[16] we have chosen to examine anatase as the support. However, to prevent transformation of anatase to rutile in the presence of CuO, it was necessary to add lanthanum oxide. Resistance changes of the TiO_2 semiconducting oxide with and without catalysts has been examined as a function of CO concentration at temperatures between 400 and 600 °C. Diffuse reflectance infrared spectroscopic analysis of adsorbed species on the metal oxide surface has been correlated with the resistance changes. Electron microscopy has provided information about the microstructure and X-ray photoelectron spectroscopy on the elemental state of the surface. A theoretical model involving the twin steps of adsorption of CO and reaction with oxygen to form CO_2 has been developed and adequately explains the change of resistance as a function of alteration of the surface characteristics by addition of dopants. This study demonstrates that understanding the nature of the gas/surface interactions at high temperatures, including a detailed knowledge of the interface chemistry, nature of defects, and the influence of additives, facilitates the design of gas sensors.

Experimental Method

Sample Preparation. The materials examined were the anatase phase of TiO_2, TiO_2/10 wt % La_2O_3 mixture, and TiO_2/10 wt % La_2O_3/2 wt % CuO mixture. The high-purity TiO_2, La_2O_3, and CuO were obtained from Aldrich Chemicals. They were ball-milled in 2-propanol for 8 h before usage.

Samples for electrical measurement were made in the thick film form. Pastes for thick films were prepared by mixing ball-milled powders with 1-heptanol solvent. These pastes were then printed on gold-grid-covered alumina substrates (1.5 cm × 1.5 cm) using a 325 mesh screen and heated in air to burn off the solvent. This treatment leaves a compact film on the substrate. Gold electrodes (0.25 mm diameter) were attached to the printed circuit on the substrate with the help of conductive gold paint (Engelhard H1109, NJ). The samples were heated to 800 °C for 8 h to ensure bonding with the substrate.

Characterization of Samples. X-ray diffraction (XRD) was performed for phase identification. The data were collected between 20° and 80° with a Scintag Pad V diffractometer, using Cu Kα radiation at 40 kV voltage and 25 mA current.

X-ray photoelectron spectroscopy (XPS) was performed with a Perkin-Elmer model 550 ESCA/Auger spectrometer.

Scanning electron microscopy was carried out on a Philips XL30 FEG SEM in secondary and backscattered electron modes. The Philips CM200 Conventional TEM as well as the CM300 FEG STEM were used for the high-resolution TEM. All microscopes were equipped with EDX detectors for chemical analysis.

Infrared measurements were made using a Bruker Instruments IFS-66s Fourier transform infrared spectrometer equipped with a globar source, KBr beam splitter, and a DTGS detector. Diffuse reflectance data were obtained using a Spectra-Tech collector/environmental chamber. The temperatures listed in this study are those set on the Spectra Tech controller and are monitored by a thermocouple on the heater element. About 200 mg of sample was placed on the heater element, and we are making the assumption that the sample attains the set temperature of the heater. The samples were heated to 400 °C for 2−4 h under dynamic vacuum to remove adsorbed water. CO was introduced into the heat-treated sample at room temperature and pumped off to a final pressure of 1−2 Torr. Subsequent temperature increases were made under this few Torr pressure. The infrared measurements were made on powdered samples, compared to the sensing measurements on thick films.

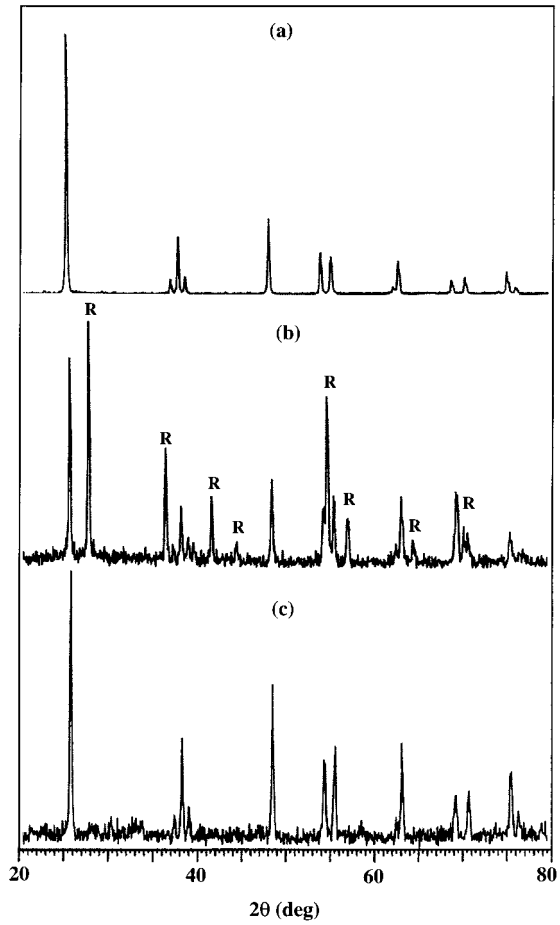

Figure 1. Powder X-ray diffraction patterns of (a) A, (b) anatase/2 wt % CuO, (c) ALC after heat treatment at 800 °C for 8 h (R-rutile phase).

Electrical Measurements. The assembly used for electrical measurements including the furnace, gas flow arrangements, and acquisition of data has been described in ref 8. The electrical resistance of the thick film samples were measured at 400, 500, and 600 °C as a function of CO concentration in a nitrogen stream containing ~1 ppm of O_2. Prior to introduction of a new dose of CO, the resistance of the sensor was allowed to reach the steady-state value (15−30 min).

Results

a. Phases of TiO_2. The parameter that determines the suitability of TiO_2 as a sensor is its change in resistance in the presence of CO. Since different phases of TiO_2 can have differing responses, we focus on the anatase phase. Since the sensor device preparation involved temperatures as high as 800 °C and resistance and spectroscopic studies were carried out at temperatures up to 600 °C, it was necessary to establish that the anatase phase was present under all experimental conditions. This was done by X-ray powder diffraction (XRD). The XRD pattern of titania (abbreviated henceforth as A) sintered at 800 °C is shown in Figure 1a and is seen to be a pure anatase phase. Titania samples mixed with 2 wt % CuO were examined after sintering at 800 °C, and the data are shown in Figure 1b. The anatase has converted partially to the more stable rutile (R) phase. To maintain the anatase phase, 10 wt % La_2O_3 was added to the TiO_2/CuO mixture. Figure 1c shows the XRD pattern of an anatase TiO_2/10 wt % La_2O_3/2 wt % CuO (abbreviated

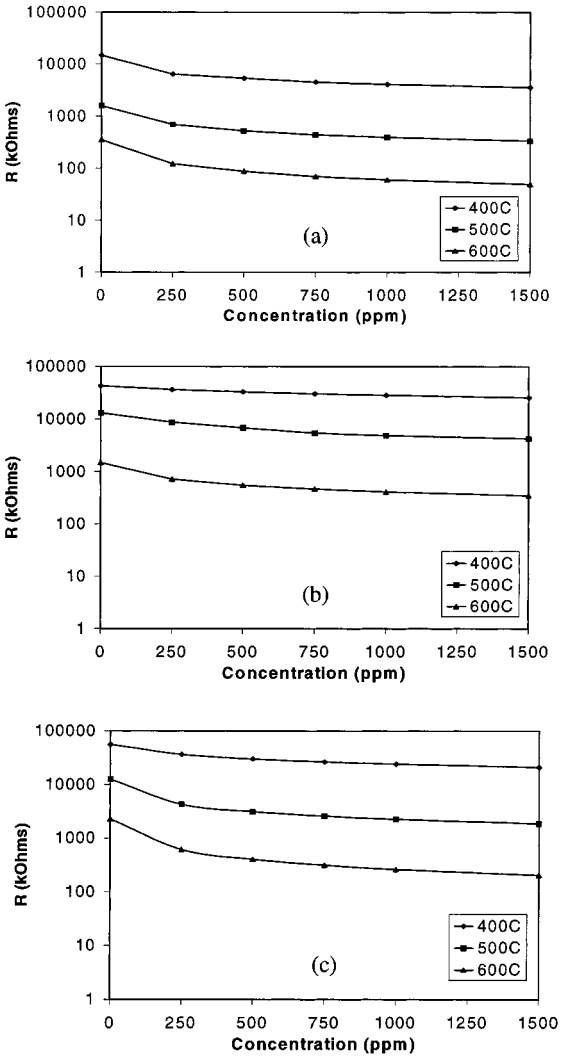

Figure 2. Resistance (R) of films of (a) A, (b) AL, and (c) ALC as a function of temperature (400−600 °C) for varying CO concentrations (0−1500 ppm). Solid lines just connect the data points.

henceforth as ALC) sintered at 800 °C and demonstrates the stabilization of the anatase phase by the addition of La_2O_3. Because the levels of La_2O_3 and CuO are sufficiently small, signals from these solids are not distinguishable in the XRD. The three samples that form the focus of this study are anatase (A), anatase/10 wt %La_2O_3 (AL), and anatase/10 wt %La_2O_3/2 wt % CuO (ALC).

b. Change in Sample Resistance upon Interaction with CO. The samples of anatase were deposited as films on an alumina substrate with a gold grid electrode. The bonding between the substrate and the anatase film was ensured by heat treatment at 800 °C. Parts a−c of Figure 2 compare the resistance changes for A, AL, and ALC as a function of CO concentration in a background of nitrogen gas over the temperature range 400−600 °C. When the relative resistances as a function of CO concentration are plotted, a better comparison of the sensitivities between the three films can be obtained. Figure 3 expresses the relative resistance changes in a normalized fashion as R/R_0, where R_0 is the resistance at 0% CO and R is the resistance in the presence of CO. From the magnitude of these resistance changes, it appears that the sensitivity to CO is dependent on the temperature of measurement; e.g., at 600 °C, the magnitude of the changes indicate that ALC > A > AL, whereas at 400 °C, the order is A > ALC > AL. Figure 4 demonstrates clearly the differences in the resistances for the

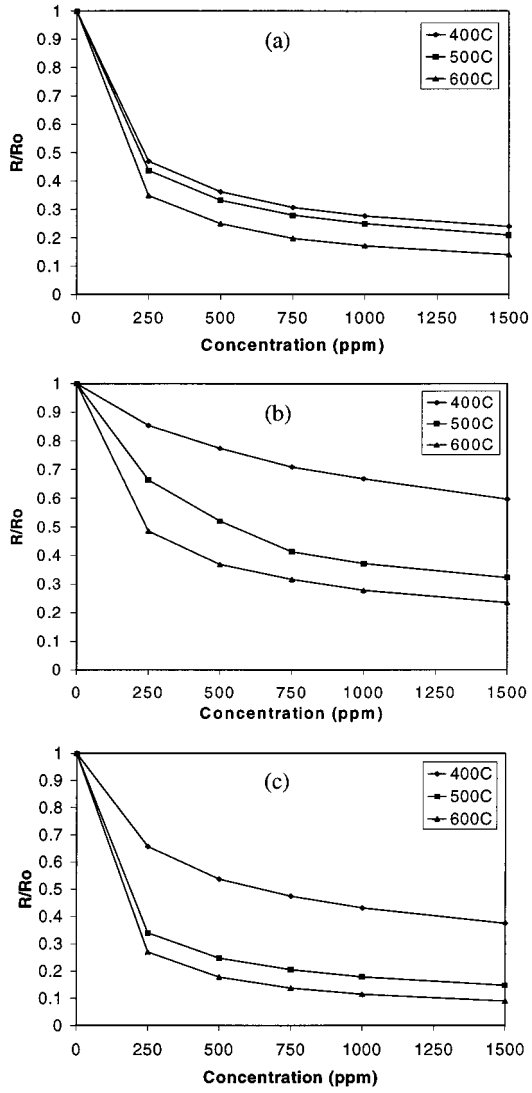

Figure 3. Relative resistances (R/R_o, R_o = resistance in background gas N_2) of films of (a) A, (b) AL, and (c) ALC as a function of temperature (400−600 °C) for varying CO concentrations (0−1500 ppm). Solid lines just connect the data points.

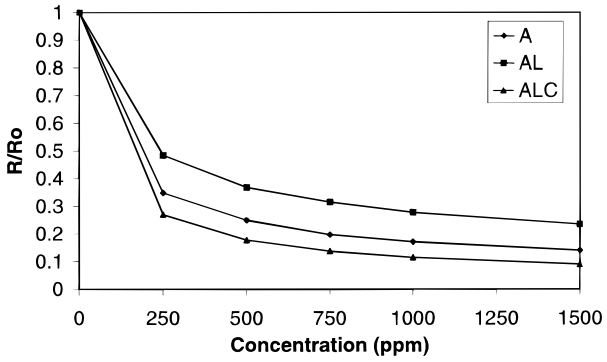

Figure 4. Comparison of the relative resistance of the films at 600 °C as a function of CO concentration. Solid lines just connect the data points.

three samples at 600 °C. Figure 5 compares the recovery of the resistance for the samples at 600 °C after exposure to 1500 ppm of CO and then turning off the CO in the gas stream. The resistance begins to rise as soon as the CO is turned off, but the eventual recovery to the resistance value before exposure to CO was incomplete for the AL sample and was considerably slower in A than in ALC.

TABLE 1: Infrared Bands of Various Titania Surfaces in the 1200−1700 cm^{-1} Region[24]

sample	temp (°C)	obsd frequencies (cm^{-1})	assignments
anatase	25	1694, 1651	bridging bidentate carbonate
	400	∼1500, 1415, 1308, 1250	carboxylate
	600	∼1500, 1415, 1308, 1250	carboxylate
anatase/La_2O_3	25	1685, 1657, 1634, 1285	bridging bidentate carbonate
	400	∼1570, 1423, ∼1300	chelating bidentate carbonate
	600	∼1600, 1423, ∼1230	chelating bidentate, monodentate carbonate
anatase/La/Cu	25	1685, 1652, 1580, 1200	bridging bidentate carbonate
	400	1685, ∼1650, 1580, ∼1300	bridging bidentate carbonate
	600	no bands observed	

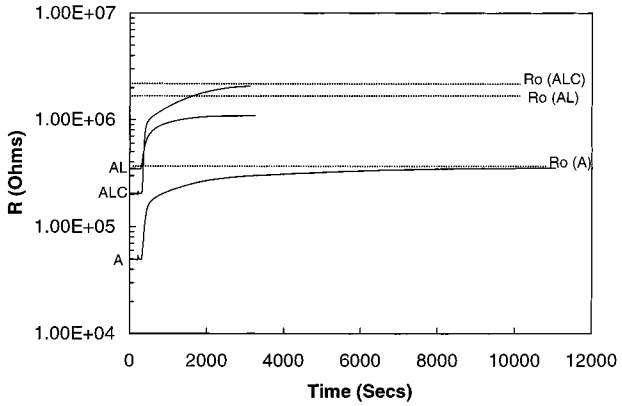

Figure 5. Dependence of the recovery of the resistance of the films as a function of time after the CO in the gas stream (N_2 with 1 ppm of O_2) is turned off.

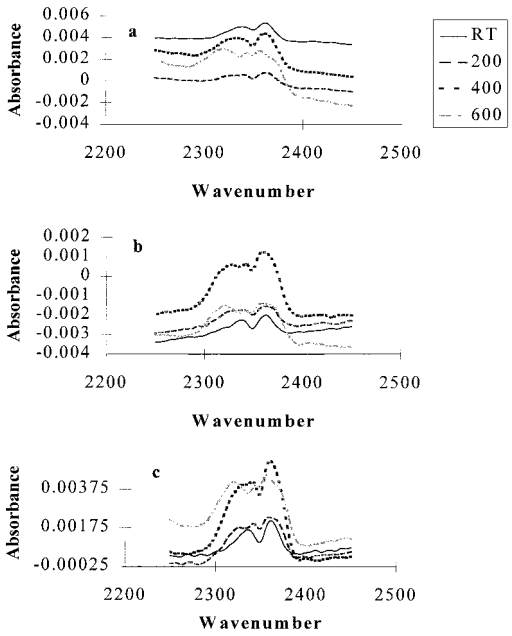

Figure 6. Infrared spectra in the C−O stretching region of CO_2: (a) A; (b) AL; (c) ALC. Intensities are in absorbance units. Temperatures of measurements are room temperature (RT), 200, 400, and 600 °C.

c. Interaction of CO with Titania by Diffuse Reflectance Infrared Spectroscopy (DRIFTS). Loosely packed powders of A, AL, and ALC were heated to 400 °C for 2−4 h, cooled to room temperature, and then exposed to 1 atm CO. The CO was then evacuated until a pressure of 2 Torr was reached. At this point, the DRIFTS of the samples was carried out from ambient temperatures to 600 °C. These data are presented in Figures 6−8, and the frequencies in the 1200−1700 cm^{-1} region are summarized in Table 1. Figure 6 shows that for all samples exposed to CO, a band around 2345 cm^{-1} due to gas-phase CO_2[17] is observed. We have plotted the *y*-axis in Figure 6 in absorbance units to provide an estimate of the gas-phase composition. The amounts of CO_2 formed tend to generally increase with temperature, although it is difficult to be quantitative, since the magnitude of the diffusely reflected light that samples the gas phase may vary with the samples.

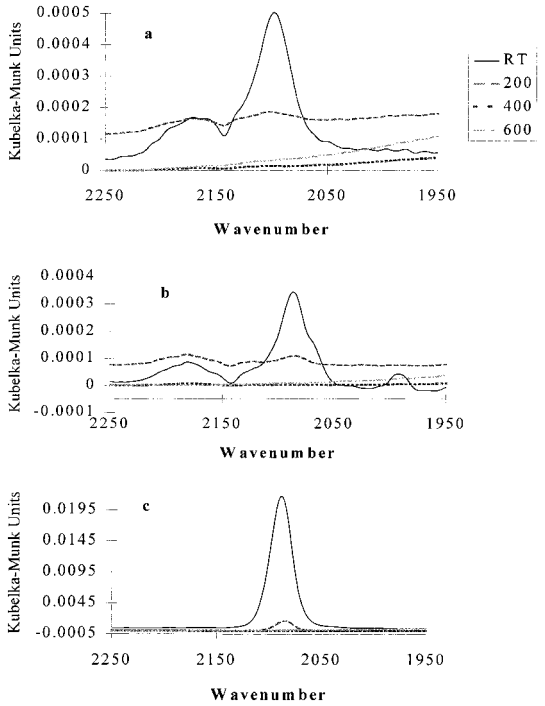

Figure 7. Infrared spectra in the C−O stretching region of CO: (a) A; (b) AL; (c) ALC. Intensities are in Kubelka−Munk units.

Figure 7 shows the spectra in the CO stretching region and is presented in Kubelka−Munk units, since adsorbed species are being examined. For all samples, there is a band around 2100 cm^{-1} arising from adsorbed CO species on the surface. Typically, physisorbed CO on titania exhibits bands around 2175−2210 cm^{-1}.[18] Considering that the present experiments were done under a vacuum of 2 Torr, the weakly held CO species are desorbed. Thus, the band at 2098 cm^{-1} is arising from chemisorbed CO species. This frequency is similar to that reported for CO on Ti^{3+} sites.[19] The weak intensity of the band indicates that the number of such Ti^{3+} defects is small and could possibly be arising from the thermal treatment prior to CO exposure. For the AL sample, the band due to adsorbed CO is even weaker and appears at 2088 cm^{-1}. However, on the ALC sample, the band at 2090 cm^{-1} is stronger by about 2 orders of magnitude compared to the A and AL samples. Infrared spectra of CO on Cu/TiO_2 is reported to show a band at 2128 cm^{-1}, significantly blue-shifted compared to the present study and attributed to CO adsorption on oxidized CuO-like sites.[20] The frequency of the CO stretching band that we observe is similar to what has been reported for CO on Cu metal on ZnO and Al_2O_3.[20,21]

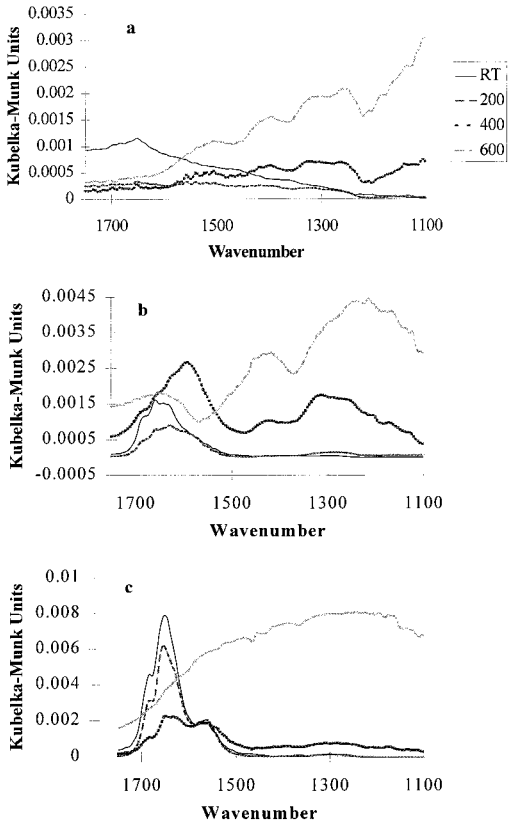

Figure 8. Infrared spectra in the carbonate stretching region: (a) A; (b) AL; (c) ALC.

Upon heating, there is a decrease in intensity of the CO band in all the samples. In the case of A and AL samples, no CO stretching band is observed beyond 200 °C. Instead, a weak band around the 2140 cm^{-1} region due to gas-phase CO with its characteristic rotational structure is observed. In the ALC sample, the band due to adsorbed CO is observed up to temperatures of 400 °C. This indicates that the magnitude of adsorption of CO onto the sensor surface follows the order ALC $\gg$ AL $\approx$ A.

The region of spectra between 1200 and 1700 cm^{-1} (Figure 8) arises from products of CO oxidation that remain on the TiO_2 surface. Several species, such as carbonates, bicarbonates, formates, and carboxylates, all show vibrational bands in this frequency region, which makes it difficult to assign the exact species. This is evident from previous assignments of bands of carbonate-like species on TiO_2. Bands at 1575, 1438, and 1359 cm^{-1} formed upon decomposition of CH_3Cl on anatase have been assigned to carbonate/bicarbonate species.[17] Studies of CO on Cu/TiO_2 report bands at 1577, 1520, 1440, 1337, and 1220 cm^{-1} attributable to carbonate-like species.[20] Bidentate carbonates on titania have been reported at 1552, 1382, and 1361 cm^{-1}.[22] Surface carboxylates on titania produced bands at 1680 and 1370 cm^{-1}.[23] A general assignment of carbonate bands on oxides suggest that bridging bidentate carbonates exhibit asymmetric stretches between 1600 and 1670 cm^{-1} and symmetric stretches around 1250 cm^{-1}, chelating bidentate carbonates have corresponding bands at 1585 and 1223 cm^{-1}, and monodentate carbonates have asymmetric stretches between 1420 and 1540 cm^{-1} and symmetric stretches around 1300 cm^{-1}.[24] In addition, carboxylates have asymmetric stretches between 1520 and 1560 cm^{-1} and symmetric stretches around 1300 cm^{-1}.[24b]

There are several general observations that can be made on the data shown in Figure 8. On the anatase surface, the bands due to carbonates are weak upon initial CO exposure. On the AL and ALC samples, strong carbonate bands are observed upon CO exposure. These bands are present on the AL sample even after heating the samples to 600 °C, whereas they disappear in the ALC samples.

In the case of anatase, the weak bidentate carbonate peaks at 1694 and 1651 cm^{-1} disappears upon heating and is replaced by bands at 1250, 1308, 1415, and 1500 cm^{-1} at temperatures exceeding 200 °C. These bands are typical of carboxylate species.[24b] Upon introduction of La into the titania samples, strong bands are observed at 1285, 1634, 1657, and 1684 cm^{-1} under ambient conditions, indicative of bridging bidentate carbonate species.[24b] Upon heating, there is a decrease in intensity of the bidentate carbonate peaks, along with a distinct appearance of a band around 1567 cm^{-1}, typical of chelating bidentate carbonate.[24b] At 600 °C, bands around 1230 and 1423 cm^{-1} typical of monocoordinated carbonates are observed. To verify that the bands being observed are not due to carbonates forming on the free La_2O_3 in the AL sample, an anatase sample was impregnated with a solution of La, with an effective loading of 1 wt % La. Similar infrared spectra as seen in Figure 8b were observed for these samples. Upon introducing Cu into the sample, the carbonate bands produced under ambient conditions are similar to that observed on the AL sample. However, the disappearance of these bands is complete at temperatures of 600 °C, suggesting there is no measurable carbonate species left on the surface, in contrast to the samples of A and AL.

d. XPS and Electron Microscopy Studies. Figure 9a shows the backscattered electron SEM micrograph of a sample of ALC. The bright spots are due to CuO and La_2O_3 particles and shows the inhomogeneous distribution of the secondary phases. A higher magnification (Figure 9b) provides a better view of the individual anatase, CuO, and La_2O_3 particles. The surface of the film is characterized by pores as large as 10 μm (Figure 9a) as well as intergranular porosity (Figure 9b). The extensive porosity is useful for promoting rapid gas penetration into the anatase film.[25] Figure 9c is a transmission electron micrograph (TEM) of individual anatase particles. The size of the anatase particles varies between 70 and 200 nm. Cu-based clusters can be seen on the outer surface of the anatase particles (as shown by arrow in Figure 9c). (Inset shows a selected area of the electron diffraction pattern of the [001] zone axis of an anatase particle). Figure 10 is a high-resolution TEM image showing a copper oxide particle (having a 10 nm thickness) attached to the surface of an anatase particle. The sample was oriented in such a way so that rows of (002) type anatase planes can be seen (spacing = 4.8 Å) as well as the (110) type planes of CuO. This micrograph does not contain definite information regarding the type of interface formed between the two materials or the existence of an orientation relationship between them. Further studies are required to clarify these issues. The film thickness at the edge of the substrate was found to be 15 μm.

To obtain information on the valence state of Cu, XPS studies were done on the sample. Figure 11 compares the X-ray photoelectron spectra of an ALC sample before and after treatment with CO at 500 °C in the Cu $2p_{3/2}$ region. Before reaction with CO, the peak in the ALC sample appears at 932.8 eV, indicative of Cu^+.[26] After the sensing reaction, the peak shifts to 932.0 eV, indicative of further reduction of the copper. It has been reported previously that photoreduction of CuO is possible in the X-ray beam, especially of small well-dispersed CuO,[14] typical of what the TEM indicates for the samples used in this study (Figure 10). This makes it difficult to deduce the

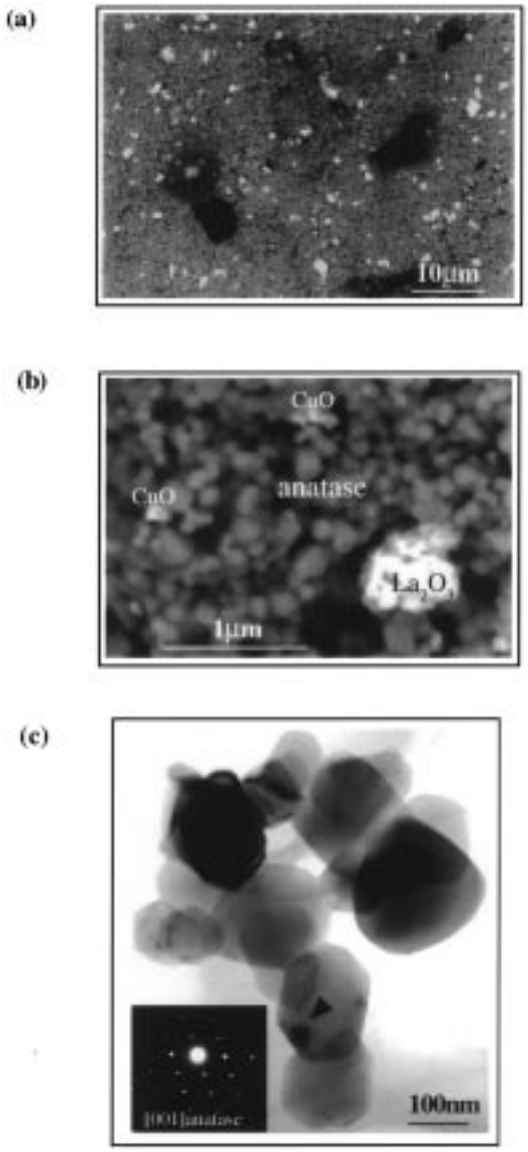

Figure 9. (a) Scanning electron micrograph taken in backscattered electron mode (BSE) showing the surface of a thick film of ALC. (b) Another BSE image showing the same area as in (a) but with higher magnification. EDX analysis has been performed to analyze the various components present in the system. (c) TEM in bright field mode showing the anatase particles of the film. Arrow indicates a copper oxide cluster surrounding the surface of the anatase particles. Inset is a selected area of the diffraction pattern of the [001] zone axis of an anatase particle.

nature of the Cu, but we note that after the sensing reaction with CO, there appears to be a reduction in the Cu binding energy.

Discussion

The dependence of the resistance of the anatase and anatase-doped samples on the amount of CO in the gas stream is of central importance in its performance as a sensor. We correlate these resistance changes with the spectroscopic data and suggest possible chemical reactions. On the basis of these correlations, we explain the role of the added lanthanum and copper oxides. The chemical reactions at the anatase surface are incorporated into a theoretical model, which provides a correlation between the resistance data and the energies associated with the adsorption of the CO on the surface and the energy associated with the reaction of CO with oxygen to form CO_2.

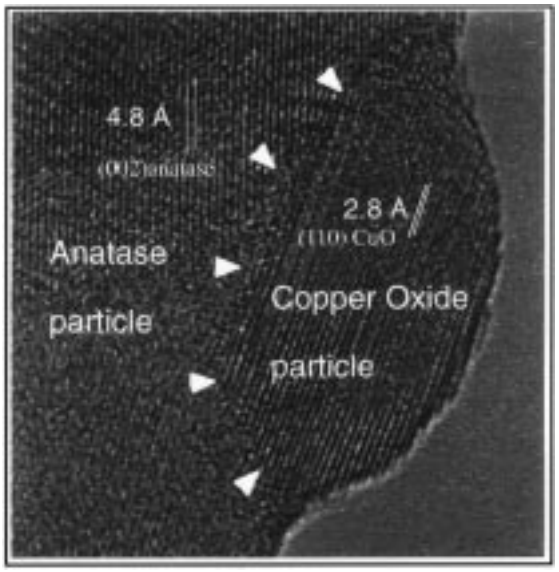

Figure 10. High-resolution TEM showing the attachment of a single copper oxide particle on the surface of an anatase particle.

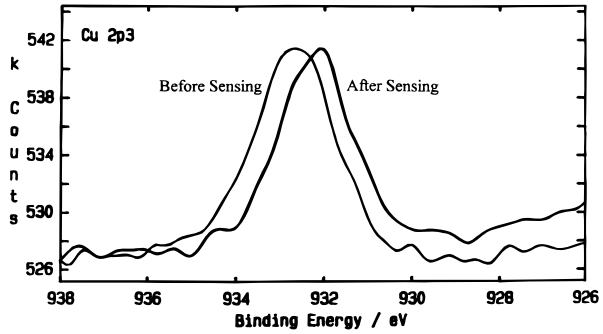

Figure 11. XPS in the $Cu3p_{3/2}$ region for ALC before and after sensing with CO.

I. Anatase to Rutile Conversion. Our objective was to examine how the resistance changes of the anatase film in the presence of CO could be enhanced by addition of catalysts, especially at temperatures around 600 °C. On the basis of literature reports that CuO on titania are good catalysts for CO oxidation, we have used CuO as an additive.[14] Temperatures as high as 800 °C are necessary to form contacts between the titania crystallites in the film as well as to bond the film to the alumina substrate used in the sensing measurements. At these temperatures, the presence of CuO led to the transformation of anatase to rutile. Previous studies have suggested that transition metals promote the transformation of anatase to rutile by diffusing into the lattice and increasing the defect concentrations that lead to bond rupture and the atomic rearrangements necessary for the transformation.[27] Sixty nm crystallites of CuO_x have been observed on TiO_2 prepared by impregnation of TiO_2 with Cu^{2+} solutions and heat treatment to 500 °C.[14] Under our conditions of heating to 800 °C, solid-state diffusion of the Cu into the anatase lattice occurs, leading to phase transformation. It is also reported in the literature that the anatase-to-rutile conversion can be retarded in the presence of rare-earth oxides.[28] Indeed, our choice of La_2O_3 was made for this reason and, as seen from Figure 1, indeed helps to stabilize the anatase structure in the presence of CuO. The anatase-to-rutile transformation is typically characterized by enhanced sintering.[29] It has been reported in the literature that CeO_2 or La_2O_3 will prevent the transformation of transition-alumina into α-alumina.[30] Alumina-

doped samples of anatase were found to have slower growth rates of crystallites upon heating.[31] Doping of La on nanometer-sized crystallites of anatase retarded the phase transformation to rutile.[32] There are several mechanisms proposed on how rare-earth elements can influence phase transformations. These include migration of the rare-earth element into interstitial sites of anatase and creation of oxygen vacancies that inhibit nucleation of rutile. Another mechanism involves the coverage of the surface by the rare-earth elements, thereby restricting grain growth. Our TEM studies do not indicate the formation of an amorphous layer of La on the anatase surface. Yet the infrared studies indicate that the presence of La increases the reactivity of the anatase surface toward CO. Also, the resistances reported in Figure 2 indicate that addition of La increases the resistance of the sample. We propose that La is attaching to the anatase surface, possibly substituting on the surface Ti sites by the following reaction:

$$La_2O_3 + {}^1/_2O_2 + 2e \rightleftharpoons 2La_{Ti}' + 4O_0^*$$

Such substitution would lead to creation of new oxygen sites on the surface as well as to an increase in resistance of the material. The presence of La on the surface of anatase particles may also prevent the Cu from diffusing into the anatase lattice, by altering the surface reactivity of the anatase. The presence of discrete CuO crystallites on TiO_2 is evident from the electron micrographs in Figures 9 and 10.

II. Correlations between Resistivity Changes and the CO Reactivity on Titania. The resistance changes of the anatase film observed upon changes in the introduction of CO are intimately related to the oxygen chemistry at the anatase surface. Figure 9a shows that the film is made up of anatase, La_2O_3, and CuO particles. Since the resistance changes being examined involve chemistry on the surface of anatase, only the La and Cu that are directly interacting with the anatase particles will play a role in influencing CO oxidation. The isolated La_2O_3 and CuO particles are not expected to play any role in the chemistry observed here.

On the basis of the literature,[6,33] several possible schemes for the oxidation reaction can be written, with the eventual result being a change in resistance, the parameter being measured.

Mechanism I

$$O_2\,(\text{gas}) \rightarrow O_2\,(\text{ads})$$

$$O_2\,(\text{ads}) + e \rightarrow O_2\,(\text{ads})^-$$

$$CO\,(\text{gas}) \rightarrow CO\,(\text{ads})$$

$$2CO\,(\text{ads}) + O_2\,(\text{ads})^- \rightarrow \text{adsorbed intermediate} \rightarrow 2CO_2\,(\text{ads}) + e$$

$$CO_2\,(\text{ads}) \rightarrow CO_2\,(\text{gas})$$

Mechanism II

$$O_2\,(\text{gas}) \rightarrow 2O\,(\text{ads})$$

$$CO\,(\text{gas}) \rightarrow CO\,(\text{ads})$$

$$CO\,(\text{ads}) + O\,(\text{ads}) \rightarrow \text{adsorbed intermediate} \rightarrow CO_2\,(\text{ads})$$

$$CO_2\,(\text{ads}) \rightarrow CO_2\,(\text{gas})$$

$$O\,(\text{ads}) \rightarrow O_2\,(\text{g}) + V_O^{2+} + 2e$$

Mechanism III

$$TiO_2 + CO\,(\text{gas}) \rightarrow TiO_2\,(CO)_{ad}$$

$$TiO_2\,(CO)_{ad} \rightarrow TiO_x\,(\text{adsorbed intermediate}) \rightarrow TiO + CO_2\,(\text{g})$$

$$Ti^{II} \rightarrow Ti^{IV} + 2e$$

$$TiO + {}^1/_2O_2\,(\text{g}) \rightarrow TiO_2$$

At high temperatures in a low-oxygen environment, titania (TiO_{2-x}) is an n-type semiconducting oxide because of the existence of a substantial concentration of O vacancies.[2] Mechanism I suggests that adsorption of oxygen at the surface defects can lead to formation of species O_2^- (and other oxygen species depending on temperature).[24b] This leads to formation of dipole charge layers and associated depletion regions at the surface of each grain. The resulting back-to-back Schottky barriers make the resistivity of the granular film much higher than that of a bulk sample. In the presence of a reducing gas such as CO, reactions at the grain surface leading to CO_2 liberate free electrons in the depletion layer, reducing the resistance at the interface and are the basis for the sensing mechanism. Mechanism II suggests reaction between CO and O (ads) and neglects charge transfers altogether. The resistance change occurs because of the correspondence between O (ads) and the electron concentration. Mechanism III involves direct reduction of Ti(IV) on the anatase surface. After CO_2 desorbs, the extra electrons associated with the reduced Ti are distributed through the lattice, resulting in a decrease in resistance. Oxygen can reoxidize the site, resulting in generation of the starting material.

The change in resistance upon introduction of CO gas stems from a combination of several factors. These include defects on the anatase surface, adsorption of oxygen, adsorption of CO, reaction of CO with oxygen on the surface to form intermediates, and desorption of CO_2 from the surface. The data that we have presented above allow us to comment on several of these features.

a. Oxygen-Related Defects. At a particular temperature, the resistance of the samples follows the order anatase/La_2O_3/CuO $\sim$ anatase/La_2O_3 > anatase. We are neglecting the effects of bulk La_2O_3 and CuO on the conductivity, since their amounts are small. The increased resistance of samples containing La can be explained as arising from substitution of La onto the titanium sites. This also leads to creation of more oxygen sites. For La-doped SnO_2 samples, stabilization of surface oxygen species has also been noted.[34]

b. Adsorption of CO at the Surface. On the basis of the intensity of the 2100 cm^{-1} band, the levels of adsorption of CO on the anatase surface is smaller than those of the AL sample, both of which are significantly lower than the Cu-containing sample. It appears that the inclusion of CuO in the composition leads to a significant increase in CO adsorption. As shown in the electron micrograph (Figure 10), we observe CuO on the titania surface. XPS data indicate that after the sample has been exposed to CO, there is a reduction in the binding energy, indicating a lower valence state of copper.[14,26] However, the samples were exposed to ambient air prior to the XPS study, and it is known that oxidation of copper can occur at room temperature,[35] so it is difficult to conclude from the XPS studies the valence state of the Cu during the sensing reaction. There have been a number of studies on the reactions of CO on CuO[36,37] that provide some clues about the nature of the Cu in the present system. Under excess of CO at high

temperatures, metallic copper is the stable phase.[38] Copper itself can act as a CO oxidation catalyst, and the order of effectiveness follows $Cu > Cu^+ > Cu^{2+}$.[38] A system that has been extensively studied as a catalyst for methanol oxidation is Cu on ZnO.[39] In this case, there is evidence based on EXAFS and XPS that the Cu is not dissolving in the ZnO phase,[40] similar to what we are proposing for Cu on anatase. For Cu/ZnO, it was found that CO chemisorption on Cu^0 was weaker than on Cu^+.[41] We propose that the significant increase in the intensity of the CO stretching band on the ALC sample compared to the A or AL sample arises from the extra sites that are produced on the reduced CuO surface.

c. Presence of Product Species on the Titania Surface. Infrared spectroscopy in the 1200−1700 cm^{-1} region provides information on the products of CO oxidation on the anatase surface. On the AL surface, the CO reacts with the surface to form bidentate carbonate species under ambient conditions. The presence of La on the surface appears to increase the reactivity of CO. With increasing temperature, the bidentate bands convert to monodentate-like species. The introduction of CuO on the anatase surface also shows formation of bidentate carbonate species at ambient temperatures. However, the important observation in the presence of CuO is that the carbonates decompose completely at the higher temperatures (600 °C).

d. Correlation between CO Sensitivities and Surface Reactivities. Both the change in the relative resistance of the anatase film upon exposure to CO and the recovery of the resistance upon turning the CO off can be related to the chemical changes occurring on the titania surfaces. The data shown in Figures 2−4 were recorded after the system reached a steady value of resistance, so it represents an equilibrium involving CO, O_2, and CO_2 adsorption, desorption, and formation. The change in relative resistances is a measure of the sensitivity toward CO detection for the three samples. There is a variation in this order depending on the temperature. At the low end of the measurements, i.e., 400 °C, the order of sensitivity is A > ALC > AL, whereas at 600 °C, the order is ALC > A > AL. The infrared spectra show that at 400 °C, there is significant amounts of carbonate species on the AL and ALC samples, whereas on the A surface, weak carboxylate peaks appear. For the AL and ALC samples, species formed by the reaction of CO with the surface-adsorbed oxygen still tie up the electrons and do not release it into the bulk, thus keeping the resistance high. On the anatase surface, there is the least amount of adsorbed species, explaining why the anatase sample shows higher sensitivity. At 600 °C, the infrared data indicate that carbonates are present on the AL samples and that there are increased carboxylates on the A sample, but no species are observed on the ALC sample, giving it the highest sensitivity. The lowest sensitivity toward CO at all temperatures is exhibited by the AL sample. Even with the lower temperature SnO_2 sensors, it has been noted that doping with La decreases sensitivity toward CO.[34]

The recovery of the samples after CO is turned off is compared in Figure 5 at 600 °C. This recovery is dependent on the oxygen present in the nitrogen stream reoccupying the adsorption sites and capturing the electrons (Mechanisms I and II) or oxidizing the Ti (Mechanism III), all of which leads to an increase in resistance of the sample. Obviously, this rate is dependent on the amount of oxygen in the stream, with recovery times becoming shorter with increasing oxygen.[6,33] However, because the resistance measurements for all three samples are done in the same background gas, the rates of recovery can be compared. The data show that the recovery is fastest in the ALC sample. The anatase sample takes about three times as long as the CuO-doped sample to recover, whereas the AL sample does not recover at 600 °C. The infrared data show that there is adsorbed species on the anatase sample, and replacement by oxygen of these species is the rate-limiting step. For the AL sample, a heat treatment to 800 °C was required to recover the resistance. The faster recovery of the anatase/La_2O_3/CuO sample is due to the fewer sites from which desorption needs to occur prior to oxygen adsorption.

The mechanism by which the presence of CuO promotes the reaction of adsorbed CO with oxygen on the anatase surface can be understood on the basis of several models in the literature. In the Cu/ZnO system, it has been proposed that the important catalytic sites are at the interface between the Cu and the oxide.[42] Similarly, the perimeter interfaces between Au and TiO_2, and Pt and SnO_2 have also been considered important sites of CO oxidation even under ambient temperature conditions.[43,44] In particular, a mechanism of CO oxidation on Au/TiO_2, based on desorption and FTIR data, suggests that CO is adsorbed on Au and migrates out toward the interface between Au and TiO_2 and reacts with the oxygen to form carbonates, whose decomposition is the rate-determining step.[45] A similar mechanism would suggest that the oxygens at the interface between the CuO and the anatase have higher reactivity with the CO.

The involvement of the carbonate species in controlling catalytic activity has been noted for Pt/SnO_2,[46] with the loss in catalytic activity being explained as arising from bicarbonate buildup blocking active sites. In the present study, the presence of CuO on the anatase surface promotes carbonate decomposition. There is a parallel here in the final step of methanol synthesis on Cu/ZnO, where a neutral methanol molecule desorbs from the surface methoxide ion. The Cu/ZnO junction is proposed to facilitate the acceptance of the electron from the methoxide ion.[42]

Thus, in the ALC sample, both La and Cu are playing several roles. La stabilizes the anatase phase and provides more oxygen sites. The presence of CuO on the anatase surface accomplishes several things. First, it increases the CO adsorption. Second, it promotes the reaction of CO with the surface oxygens at the CuO/anatase interface. Third, CuO helps in the desorption of the CO_2. This makes it possible to achieve higher sensitivities and faster recovery than anatase at the highest temperatures.

III. Modeling the Surface Reactivity of Titania. To model the change in resistance of the different anatase-based materials, several stages in the sensor response need to be described, including the gas adsorption and reaction process on the surface of the TiO_2 grains, the resulting change in grain boundary resistance at the interface between the grains, and the conduction process through the granular composite. We consider the application of a recently proposed model,[47] which contains the simplest features of the sensing process. In particular, the basic chemistry occurring at the anatase surface is described in terms of energy levels characterizing the chemisorption of CO, the reaction with oxygen on the surface, and the desorption of CO_2. The free charge produced in the reactions is assumed to modify the effective conductivity of the interfacial grain boundary and surface depletion layer of the grain.[48,49] Finally, the conduction process is modeled by electrical percolation through the weakly sintered granular composite. The effect of the dopant additions in AL and ALC samples is taken into account by modifications of the energy levels characterizing the surface reactions. For simplicity, we assume that properties such as the bulk conductivity of the TiO_2 remain unchanged by the doping. These

assumptions appear reasonable in the present experiments, although the model may be readily extended to the more general case.

The presence of an ionized oxygen layer on the surface of an n-type oxide grain leads to carrier depletion in a region near the surface that is highly resistive compared to the bulk interior.[50] If the grains are small in size compared to the depletion layer width, the high-resistivity region may extend throughout the grain. A microscopic treatment of the surface impedance involves consideration of back-to-back Schottky barriers at the interface between two grains. The impedance may be temperature-dependent and, in some cases, also nonlinear.[47] In general, the surface impedance depends on details of the metal oxide band structure and adsorbed surface oxygen species (e.g., O^-, O^{2-}, O_2^-). However, under the conditions of controlled ambient nitrogen atmosphere of the experiments considered here, the barrier height may reasonably be expected to remain constant. In addition, it is mainly the O^- species that defines the low conductivity region at the working temperatures of the sensor.[51] Therefore, in the present work we use a simpler approach to characterize the essential features of the interface. We associate a high conductivity with the interior region of the grain and a constant low conductivity with the depletion layer region near the surface of the oxide grains generated by the surface O^- layer.

The essential behavior of the effective conductivity of such a two-component medium may be reasonably described by an effective medium theory that requires fluctuations in the local electric polarization to vanish.[52] In the present case, the high- and low-conductivity components are not randomly distributed, but instead the low-conductivity (depletion and grain boundary) regions surround the high-conductivity interior regions. The effective conductivity σ_{eff} for such a two-component composite in which the insulating component coats the conducting one is given by the unsymmetrical effective medium theory[47,52]

$$(\sigma_{\text{eff}} - \sigma_{\text{g}})^3/\sigma_{\text{eff}} = (1 - f_{\text{g}})^3(\sigma_{\text{i}} - \sigma_{\text{g}})^3/\sigma_{\text{i}} \qquad (1)$$

where σ_{i} and σ_{g} are the conductivities of the insulating interface and conducting grain components, respectively, and f_{g} is the volume fraction of the highly conducting or the nondepleted region of the sensor determined by the carriers intrinsically present in the n-type oxide, plus those released through the surface CO_2 reaction process. The fraction of the insulating region $(1 - f_{\text{g}})$ is characterized by the carriers depleted by surface O^-. In the TiO_{2-x} sensor, the electron carrier fraction f_{g} is determined by the oxygen deficiency x, the surface-adsorbed oxygen concentration (represented here as O^-_{ads}), and the electrons produced in the CO_2 reaction:

$$f_{\text{g}} = \frac{2x - [\text{O}^-_{\text{ads}}] + [\text{e}_{\text{reac}}]}{2x} \qquad (2)$$

where x is assumed to remain constant during the sensing measurement taken in a CO/N_2 ambient devoid of oxygen.

The number of electrons returned to the depletion layer through CO oxidation and the amount of surface O^- are determined using standard kinetic methods. We find that it is necessary to include at least two energy levels in the kinetics, as one energy level modeling yields little temperature dependence of the effective conductivity. The two equilibrium reactions contributing to the overall mechanism are

$$\text{CO (g)} + \text{O}^-_{\text{ads}} \underset{k_{\text{ar}}}{\overset{k_{\text{af}}}{\rightleftarrows}} \text{CO}_{\text{ads}}\cdot\text{O}_{\text{ads}} \underset{k_{\text{ir}}}{\overset{k_{\text{if}}}{\rightleftarrows}} \text{CO}_{2,\text{ads}} + \text{e}_{\text{reac}}^- \qquad (3)$$

We note that the number of CO_2 leaving the oxide surface equals the number of free electrons produced in the reaction. Therefore, calculation of $[CO_2]$ determines the released electrons. In addition, the following conservation law governs the occupation of surface sites:

$$[\text{O}^-_{\text{ads}}] + [\text{CO}_{\text{ads}}\cdot\text{O}^-_{\text{ads}}] + [\text{CO}_{2,\text{ads}}] = [\text{S}_{\text{O}}] \qquad (4)$$

where $[S_O]$ is the concentration of adsorption sites on the oxide surface. By use of standard chemical kinetic methods, the steady-state surface concentrations $[CO_2]$ and $[O^-_{\text{ads}}]$ are found to be[53,54]

$$[\text{CO}_{2,\text{ads}}] = \frac{k_{\text{af}}}{k_{\text{ar}}}\frac{k_{\text{if}}}{k_{\text{ir}}}\frac{[\text{CO (g)}][\text{S}_{\text{O}}]}{1 + \left(1 + \frac{k_{\text{if}}}{k_{\text{ir}}}\right)\frac{k_{\text{af}}}{k_{\text{ar}}}[\text{CO(g)}]} \qquad (5)$$

$$[\text{O}^-_{\text{ads}}] = \frac{[\text{S}_{\text{O}}]}{1 + [1 + (k_{\text{if}}/k_{\text{ir}})](k_{\text{af}}/k_{\text{ar}})[\text{CO (g)}]]} \qquad (6)$$

Ratios of the forward and reverse reaction rates for equilibrium reactions may generally be written in terms of the appropriate partition functions, where ΔE is the difference between the activation energies of the forward and reverse reactions ($E = E_{\text{f}} - E_{\text{r}}$).

$$\frac{[\text{product}]}{[\text{reactant}]} = \frac{F_{\text{product}}}{F_{\text{reactant}}}\,\text{e}^{\Delta E/(RT)} \qquad (7)$$

The partition functions F_{product} and F_{reactant} are related to the frequencies of the forward and reverse reactions and yield important characteristics of the sensor. We will investigate the time response in greater detail in a separate publication. In evaluating the equilibrium properties of the sensor, we note that the partition function ratio $F_{\text{product}}/F_{\text{reactant}}$ of the adsorption gas/surface reaction is λ^3, where λ is the Debye wavelength (or the mean thermal wavelength) and for CO is 1.19×10^{-11} m, while the partition function ratio is unity for the surface reaction.

Denoting by E_{a} and E_{i} the energies of the two respective reactions in eq 3, the reaction rates in eqs 5 and 6 become[55]

$$k_{\text{af}}/k_{\text{ar}} = \lambda_{[\text{CO(g)}]}{}^3 \exp[E_{\text{a}}/(k_{\text{B}}\text{T})] \qquad (8)$$

$$k_{\text{if}}/k_{\text{ir}} = \exp[-E_{\text{i}}/(k_{\text{B}}T)] \qquad (9)$$

A larger value of E_{a} corresponds to a more energetically favorable environment for adsorption of the CO gas. Conversely, the resistance drop is less for a larger value of E_{i}, which makes it less likely for the CO_2 to form and escape and contribute an electron to the depletion layer. We will assume that the nature of the oxygen species remains invariant with temperature.

By use of eqs 8 and 9 in eqs 5 and 6 for the gas concentrations, both the released electron concentration and surface O^- concentration are determined and eqs 2 and 1 may be solved for the effective conductivity. Figure 12 compares the conductivities predicted by the effective medium model with those measured experimentally in the anatase sample at temperatures of 400, 500, and 600 °C. Similar fits for the doped anatase samples allow a determination of the energies E_{a} and E_{i} for all samples. The values given in Table 2 indicate that the main effect of the CuO is to facilitate the chemisorption of CO gas on the anatase surface, as witnessed by the change in value of the adsorption energy E_{a}. The adsorption energies of CO follow the order ALC > A and are consistent with the

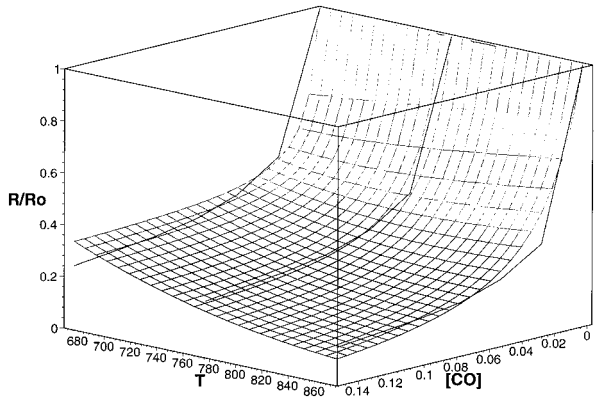

Figure 12. Calculated relative resistances (lighter grid) using effective medium theory of an anatase film compared to experimental data (dark lines) for temperatures 400, 500, and 600 °C (temperature scale in figure is in units of kelvin, and CO concentration in ppm/10^4).

TABLE 2: Energy Values (in eV) for Titania-Based Sensors[a]

	anatase	anatase/La_2O_3	anatase/La_2O_3/CuO
E_a	0.34	0.37	0.39
E_i	0.24	0.28	0.25

[a] Energy values given in electronvolts (eV).

experimental results. Also, the formation of the CO_2 is promoted in the Cu-containing sample, in agreement with the spectroscopic data.

Conclusion

The resistivity change of titania due to surface reaction of CO with adsorbed oxygen can be used to sense the presence of CO at high temperatures. The problem with this material is that recovery of the resistance of the material upon turning off CO is slow, owing to the strongly held carboxylates formed on the surface. A catalyst material such as CuO was examined but led to the transformation of anatase to rutile. This phase change could be retarded by addition of La_2O_3 to the sample. The presence of La on anatase leads to the formation of oxygen defect sites, which lead to enhancement of the number of oxygen species, and thereby increases the reactivity of CO with the surface. However, the products of this reaction are carbonate species that are not decomposed readily, thus blocking off oxygen adsorption sites and leading to poor recovery of the sensor in the absence of CO. The addition of both La_2O_3 and CuO enhances the adsorption of CO, reactivity of the surface toward CO, and the desorption of the CO_2. Thus, the anatase system can be converted to an efficient CO sensor in terms of both reactivity of CO on the surface as well as the recovery of the sensor after the CO is turned off by the presence of both La_2O_3 and CuO.

Acknowledgment. We acknowledge funding by NSF Grants EEC-9523358 and DMR-9503429.

References and Notes

(1) (a) *New Concepts in Selective Oxidation over Heterogeneous Catalysts*; Centi, G., Misono, M., Eds.; Catalysis Today 41; Elsevier: Amsterdam, 1988; p 1. (b) Poulston, S.; Price, N. J.; Weeks, C.; Allen, M. D.; Parlett, P.; Steinberg, M.; Bowker, M. *J. Catal.* **1998**, *178*, 658.

(2) (a) McAleer, J. F.; Moseley, P. T.; Norris, J. O. W.; Williams, D. E. *J. Chem. Soc., Faraday Trans. 1* **1987**, *83*, 1323. (b) Vancu, A.; Ionescu, R.; Barsan, N. Chemoresistive Gas Sensors. In *Thin Film Sensors*; Ciureanu, R., Middelhoek, S., Eds.; Institute of Physics Publishing: Philadelphia, 1992.

(3) (a) Ikohura, K.; Watson, J. *The Stannic Oxide Gas Sensor*; CRC Press: Boca Raton, FL, 1994. (b) Watson, J.; Ihokura, K.; Coles, G. *Inst. Phys. Meas. Sci. Technol*. **1993**, *4*, 711.

(4) Koltsakis, G. C.; Stamatelos, A. M. *Proc.—Inst. Mech. Eng., Part D* **1995**, *209*, 171.

(5) Moseley, P. T.; Crocker, A. J. *Sensor Materials*; Institute of Physics Publishing: Philadelphia, 1996.

(6) (a) Logothetis, E. M. *Ceram. Process. Eng. Sci*. **1980**, *1*, 281. (b) Logothetis, E. M.; Park, K.; Meitzler, A. H.; Laud, K. R. *Appl. Phys. Lett*. **1975**, *26*, 209.

(7) (a) Tan, Y.; Tan, T. C. *Sens. Actuators B* **1995,** *28*, 113. (b) Miura, N.; Raisen, T.; Lu, G.; Yamazoe, N. *J. Electrochem. Soc*. **1997**, *144*, L198.

(8) Birkefeld, L. D.; Azad, M. A.; Akbar, S. A. *J. Am. Ceram. Soc*. **1992**, *75*, 2964.

(9) Tien, T. Y.; Stadler, H. L.; Gibbons, E. F.; Zamanidis, P. J. *Ceram. Bull*. **1975**, *54*, 280.

(10) Micheli, A. L. *Am. Ceram. Soc. Bull.* **1984**, *63*, 694.

(11) Harris, L. A. *J. Electrochem. Soc*. **1980**, *127*, 2657.

(12) (a) Bond, G.; Molloy, L.; Fuller, M. J. *J. Chem. Soc., Chem. Commun*. **1975**, 796. (b) Huck, R.; Bottger, U.; Kohl, D.; Heiland, G. *Sens. Actuators* **1989**, *17*, 355.

(13) Prasad, R.; Kennedy, L. A.; Ruckenstein, E. *Combust. Sci. Technol*. **1980**, *22*, 271.

(14) Larsson, P.; Andersson, A.; Wallenberg, L. R.; Svensson, B. *J. Catal*. **1996**, *163*, 279.

(15) Cox, P. A. *Transition Metal Oxides*; Clarendon Press: Oxford, 1992.

(16) Deo, G.; Turek, A. M.; Wachs, I. E.; Machej, T.; Haber, J.; Das, N.; Eckert, H.; Hirt, A. M. *Appl. Catal.* **1992**, *A91*, 27.

(17) Wong, J. C. S.; Linsebigler, A.; Lu, G.; Fan, J.; Yates, J. T. *J. Phys. Chem*. **1995**, *99*, 335.

(18) (a) Garrone, E.; Bolis, V.; Eubini, B.; Morterra, C. *Langmuir* **1989**, *5*, 892. (b) Morterra, C. *J. Chem. Soc., Faraday Trans. 1* **1988**, *84*, 1617.

(19) Busca, G.; Saussey, H.; Saur, O.; Lavalley, J. C.; Lorenzelli, V. *Appl. Catal*. **1985**, *14*, 245.

(20) Bocuzzi, F.; Chiorino, A. *J. Phys. Chem*. **1996**, *100*, 3617.

(21) Padley, M. B.; Rochester, C. H.; Hutchins, G. J.; King, F. *J. Catal*. **1994**, *148*, 438.

(22) Marwood, M.; Doepper, R.; Renken, A. *Appl. Catal. A.* **1997**, *151*, 223.

(23) Baraton, M.-I. *Sens. Actuators B* **1996**, *31*, 33.

(24) (a) Dixit, L.; Prasada Rao, T. S. R. *Appl. Spectrosc. Rev.* **1996**, *31*, 369. (b) Moseley, P. T.; Williams, D. E. In *Techniques and Mechanisms in Gas Sensing*; Moseley, P. T., Norris, J. O. W., Williams, D. E., Eds.; Adam Hilger: Bristol, 1991; p 46.

(25) Logothetis, E. M.; Kaiser, W. J. *Sens. Actuators* **1983**, *4*, 333.

(26) Wollner, A.; Lange, F.; Schmelz, H.; Knozinger, H. *Appl. Catal. B.* **1993**, *94*, 181.

(27) (a) Iida, Y.; Ozaki, S. *J. Am. Ceram. Soc.* **1961**, *44*, 120. (b) Mackenzie, K. J. D. *Trans. J. Br. Ceram. Soc.* **1975**, *71*, 77.

(28) Hishita, S.; Mutoh, I.; Koumoto, K.; Uanagida, H. *Ceram. Int.* **1983**, *9*, 61.

(29) Kumar, K.-N. P.; Keizer, K.; Burggraff, A. J. *J. Mater. Sci. Lett.* **1994**, *13*, 59.

(30) Ozawa, M.; Kinura, M.; Isogai, A. *J. Mater. Sci. Lett.* **1990**, *9*, 291.

(31) Xing, D.; Liu, L.; Ma, X.; Qi, Z.; He, Y. *J. Mater. Sci. Lett.* **1994**, *13*, 462.

(32) Gopalan, R.; Lin, Y. S. *Ind. Eng. Chem. Res*. **1995**, *34*, 12289.

(33) Coles, G. S. V.; Williams, G.; Smith, B. *J. Phys. D.: Appl. Phys.* **1991**, *24*, 633.

(34) Fukui, K.; Nakane, M. *Sens. Actuators B* **1995**, *24*−*25*, 486.

(35) Del Arca, M.; Caballero, A.; Malet, P.; Rives, V. *J. Catal.* **1988**, *113*, 120.

(36) Domagala, M. E.; Campbell, C. T. *Catal. Lett.* **1991**, *9*, 65.

(37) Choi, K. I.; Vannice, M. A. *J. Catal.* **1991**, *131*, 22.

(38) Jerrigan, G. C.; Somorjai, G. A. *J. Catal*. **1994**, *147*, 567.

(39) Chinchen, G. C.; Waugh, K. C. *J. Catal.* **1986**, *97*, 280.

(40) Fleisch, T. H.; Mieville, R. L. *J. Catal.* **1986**, *97*, 284.

(41) Didiziulis, S. V.; Butcher, K. D.; Cohen, S. L.; Solomon, E. I. *J. Am. Chem. Soc.* **1989**, *111*, 7110.

(42) Frost, J. C. *Nature* **1988**, *334*, 577.

(43) Iizuka, Y.; Fujiki, H.; Yamauchi, N.; Chijiiwa, T.; Arai, S.; Tsubota, S.; Haruta, M. *Catal. Today* **1997**, *36*, 115.

(44) Sheintuch, M.; Schmidt, J.; Lecthman, Y.; Yahav, G. *Appl. Catal.*. **1989**, *48*, 55.

(45) Haruta, M.; Tsubota, A.; Kobayashi, T.; Kageyama, H.; Genet, M. J.; Delman, B. *J. Catal*. **1993**, *144*, 175.

(46) Schryer, D. R.; Upchurch, B. T.; Sidney, B. D.; Brown, K. G.; Hoflund, G. B.; Herz, R. K. *J. Catal.* **1991**, *130*, 314.

(47) Chwieroth, B. S.; Patton, B. R; Wang, Y. Conduction and Gas Surface Reaction Modeling in TiO_{2-x} CO Gas Sensors. Preprint.

(48) Shimizu, Y.; Nakamura, Y.; Egashira, M. *Sens. Actuators B* **1993**, *13*−*14*, 128.

(49) Saito, S.; Miyayama, M.; Koumoto, K.; Yanagida, H. *J. Am. Ceram. Soc.* **1985**, *68*, 40.

(50) Chang, S. C. Sensing Mechanisms in Thin Film Tin Oxide. In *Chemical Sensors*, Proceedings of the International Meeting, Fukuoka, Japan, September 19−22, 1983; Seiyama, T., Fueki, K., Shiokawa, J., Suzuki, S., Eds. Analytical Chemistry Symposia 17; Elsevier: Amsterdam, 1983; p 78.

(51) Harrison, P. G.; Willett, M. J. *J. Chem. Soc., Faraday Trans. 1* **1989**, *85*, 1921.

(52) (a) Bruggeman, D. A. G. *Ann. Phys. (Leipzig)* **1935**, *24*, 636. (b) Landauer, R. Electrical Conductivity in Inhomogeneous Media. *AIP Conf. Proc.* **1977**, *40*, 2.

(53) Adamson, A. W. *Physical Chemistry of Surfaces*, 5th ed.; Wiley & Sons: New York, 1990.

(54) Steinfeld, J.; Francisco, J.; Hase, W. *Chemical Kinetics and Dynamics*; Prentice Hall: New York, 1989.

(55) Laidler, K. *Chemical Kinetics*; McGraw-Hill: New York, 1987.